

# Convergence of Electronic Structure with the Size of the QM Region: Example of QM/MM NMR Shieldings

Denis Flraig, Matthias Beer, and Christian Ochsenfeld\*

Theoretical Chemistry, University of Munich (LMU), Butenandtstrasse 7, D-81377 München, Germany

 Supporting Information

**ABSTRACT:** The influence of the chemical environment on NMR shifts of a central molecular region is studied for several biomolecular and supramolecular systems. To investigate the long-range effects, we systematically increase the QM region until the changes of the NMR shielding tensor are negligible for the considered nuclei; that is, convergence with the selected QM size is reached. To reach size convergence, QM regions with up to about 1500 atoms and 15 000 basis functions are treated by our density matrix-based linear-scaling coupled perturbed self-consistent field methods. The results also provide insights into the locality and convergence of the electronic structure. Furthermore, we demonstrate to what extent the inclusion of the chemical environment as partial point charges within a hybrid QM/MM approach improves the convergence behavior. In addition, some benchmark data on NMR accuracies are provided using various ab initio methods.

## 1. INTRODUCTION

Assigning NMR spectra by means of quantum chemical methods has become a useful tool for gaining insights into structure for a wide range of chemical systems (for an overview, see for example refs 1, 2, and references therein). With linear-scaling methods for the calculation of NMR shieldings at Hartree–Fock (HF) and Density Functional Theory (DFT) levels,<sup>3–5</sup> molecules in size ranges of 1000 atoms can be studied on simple workstation computers. In dense systems, for example, solvated biomolecular systems, size ranges of 1000 atoms are often quickly reached, starting from a central molecule region of interest and including more and more of the environment.

To account for the environment even more efficiently, we recently presented a new method that allows for sublinear scaling in the rate-determining steps of the ab initio calculation of NMR chemical shifts for selected nuclei.<sup>6</sup> In this way, for a typical range of systems with about 500–1000 atoms, another order of magnitude of speedup is achieved (while the speedup becomes of course larger with system size). The key feature of the sublinear scaling scheme is a reformulation of the response equations suitable for exploiting the locality and a reliable truncation of environmental effects.

Another (complementary) approach is to account for all long-range interactions by means of hybrid QM/MM schemes that have been well established over the last decades (see, for example, refs 7–10 for an overview). Splitting the total system into a QM and MM subsystem within a QM/MM scheme implies, of course, that the required QM size for a desired accuracy can be estimated in advance. While there have been several interesting studies on the influence of the QM-region size on QM/MM results (see, for example, refs 11–13), a systematic study for systems with more than 1000 QM atoms became only possible by the combination with linear scaling schemes.<sup>14</sup>

In the present work, we combine our linear scaling methods for the calculation of nuclear shielding tensors<sup>3–5</sup> at

Hartree–Fock and DFT levels with the QM/MM approach formulated by Cui and Karplus<sup>15</sup> to investigate the convergence of pure QM and QM/MM NMR shifts upon increasing the QM size. The convergence results not only provide important insights for calculating NMR shieldings, but can also be seen in a more general fashion as probes for the locality and convergence of the electronic structure itself. Here, we present convergence results for a variety of representative molecular systems.

## 2. QM/MM THEORY FOR THE CALCULATION OF NMR SHIELDINGS

**2.1. GIAO-SCF Approach.** We begin with a brief survey of basic principles for the GIAO-SCF approach to calculate isotropic NMR shieldings as required for the present study. The chemical shielding tensor  $\sigma_N^{ij}$  at Hartree–Fock or KS-DFT is given by

$$\sigma_N^{ij} = \sum_{\mu\nu} P_{\mu\nu} \frac{\partial^2 h_{\mu\nu}}{\partial B^i \partial m_N^j} + \sum_{\mu\nu} \frac{\partial P_{\mu\nu}}{\partial B^i} \frac{\partial h_{\mu\nu}}{\partial m_N^j} \quad (1)$$

and the gauge-origin problem may be overcome by introducing gauge including atomic orbitals (GIAO<sup>16–18</sup>). Recently, we introduced the density matrix-based Laplace-transformed coupled perturbed self-consistent field approach (DL-CPSCF) that allows one to determine  $P^{B^i}$  within an entirely density-based formulation (using a Laplace transformation with  $\tau$  Laplace points  $\alpha$  and matrix exponentials):<sup>5</sup>

$$P_{n+1}^{B^i} = \overbrace{\sum_{\alpha} \omega_{\alpha} \left\{ e^{-t_{\alpha} QF} Q \right\} \cdot b_n^{B^i} \cdot \left\{ e^{t_{\alpha} PF} P \right\}}^{P_{vo,n}^{B^i}} - \left( P_{vo,n}^{B^i} \right)^T - PS^{B^i}P. \quad (2)$$

**Received:** January 20, 2012

**Published:** June 21, 2012



Here,  $n$  denotes the iteration index,  $\mathbf{Q}$  and  $\mathbf{P}$  are the virtual and occupied one-particle density matrices, and  $\mathbf{b}_n^{B^i}$  is determined by

$$\mathbf{b}_n^{B^i} = \mathbf{S}^{B^i} \mathbf{P} \mathbf{F} - \mathbf{F}_n^{B^i} \mathbf{P} \mathbf{S} \quad (3)$$

$\mathbf{F}$  and  $\mathbf{S}$  are the Fock (Kohn–Sham) and overlap matrix, respectively, and the notation  $\mathbf{M}^{B^i}$  refers to the matrix of partial derivatives with respect to  $B^i$  of the corresponding matrix  $\mathbf{M}$ . The matrix  $\mathbf{F}_n^{B^i}$  is the sum of one-electron part  $\mathbf{h}^{B^i}$  and two-electron part  $\{\mathbf{G}[\mathbf{P}]\}_n^{B^i}$ :

$$\mathbf{F}_n^{B^i} = \mathbf{h}^{B^i} + \{\mathbf{G}[\mathbf{P}]\}_n^{B^i} = \mathbf{h}^{B^i} + \mathbf{G}^{B^i}[\mathbf{P}] + \mathbf{G}[\mathbf{P}_n^{B^i}] \quad (4)$$

**2.2. QM/MM Coupling.** The following paragraph shortly classifies different QM/MM approaches and recapitulates the derivation by Cui and Karplus<sup>15</sup> in the context of our DL-CPSCF formulation.<sup>5</sup> In principle, the coupling of QM and MM may be formulated in both an additive and a subtractive way (see, for example, ref 7). The present work is based on the additive formulation of system partitioning into a QM and an MM part:

$$\hat{H}_{\text{tot}} = \hat{H}_{\text{QM}} + \hat{H}_{\text{MM}} + \hat{H}_{\text{QM/MM}} \quad (5)$$

Commonly, a hierarchy of three models is distinguished: the mechanical, electrostatic, and polarizable embedding.<sup>8</sup> While within the mechanical embedding the term  $\hat{H}_{\text{QM/MM}}$  is only represented by the conventional MM distributions for bonded, van-der-Waals, and classical electrostatic interactions between the QM and MM subsystem, the higher-level embedding schemes treat the electrostatic contribution of the Hamiltonian  $\hat{H}_{\text{QM/MM}}$  within the QM theory, which is highly relevant for ab initio calculations of shielding tensors for the QM atoms. The electrostatic interaction of QM electrons with the MM subsystem can be added to the QM core Hamiltonian  $\hat{h}$  and is described for the present study as Coulombic interaction with partial charges centered at the MM nuclei as has become most common, although schemes based on higher order multipole terms have also been derived (see, for example, refs 19, 10, and references therein):

$$\tilde{h}_{\text{QM/MM}} = \hat{h}_{\text{QM}} + \sum_{\text{C}}^{N_{\text{MM}}} -\frac{Q_{\text{C}}}{r_{\text{C}}} \quad (6)$$

Here  $Q_{\text{C}}$  denotes an MM partial charge (as a multiple of absolute electron charge in atomic units), and  $r_{\text{C}}$  is the distance of a QM electron to the external charge.

Because of the modified core Hamiltonian  $\tilde{h}$ , the SCF procedure yields a modified density matrix  $\tilde{\mathbf{P}}$ , and by replacing  $\mathbf{P}$  with  $\tilde{\mathbf{P}}$ , the diamagnetic contribution (first term) of eq 1 is changed. Moreover, the paramagnetic contribution (second term) in eq 1 is changed, because the incorporation of external point charges influences the solutions  $(\partial/\partial B_i)P_{\mu\nu}$  of the DL-CPSCF procedure. Because the point charges contribute to the one-electron integral derivative,  $\mathbf{h}^{B^i}$  needs to be substituted by  $\tilde{\mathbf{h}}^{B^i}$  with

$$\tilde{h}_{\mu\nu}^{B^i} = h_{\mu\nu}^{B^i} - \sum_{\text{C}}^{N_{\text{MM}}} Q_{\text{C}} \left\{ \underbrace{\left\langle \frac{\partial}{\partial B^i} \mu | r_{\text{C}}^{-1} | \nu \right\rangle}_{V_{\mu\nu}^{B^i}} + V_{\mu\nu}^C \right\}, \quad (7)$$

yielding modified matrices  $\tilde{\mathbf{F}}_n^{B^i}$  (via eq 4),  $\tilde{\mathbf{b}}_n^{B^i}$  (via eq 3), and consequently  $\tilde{\mathbf{P}}_{n+1}^{B^i}$  (via eq 2).

### 3. OUTLINE OF THE STUDY

Before the detailed discussion of system setups and results in sections 4 and 5, the key aspects of our approach for studying convergence with QM size are outlined in the following.

Figure 1 illustrates the approach for studying the convergence behavior with the size of the QM region. Starting

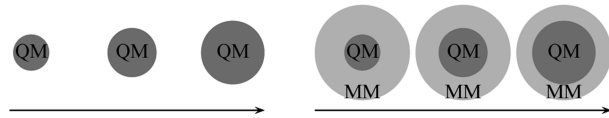


**Figure 1.** Scheme for the convergence study. Left: Pure QM calculations with increasing QM size upon convergence. Right: QM/MM calculations with increasing size upon convergence, where the MM subsystem comprises the remaining part of the molecular system.

from a central molecular region of interest (e.g., the solute), the QM cutouts are systematically increased until changes of isotropic shieldings drop below a nucleus specific criterion (see section 5). For each QM size, the remaining part of the molecular system is eliminated completely in case of pure QM calculations or incorporated as MM subsystem in case of QM/MM calculations. The size of the QM part is defined by a distance criterion, hereafter denoted as QM cutoff distance  $r$ , which has the following meaning: A molecule (or residue) of the environment is designated for the QM part, if any atom of the molecule (or residue) is nearer than the QM cutoff distance  $r$  to any of the atoms of the central molecular region of interest. By this, the QM cutouts emulate the shape of the central molecular region, and we aim for an optimal convergence behavior with respect to  $r$ , that is, lowest deviations for a given number of QM atoms. For the QM and MM partitioning, covalent bond cleavage at the QM/MM border is avoided, if possible (e.g., by including or eliminating entire solvent molecules at the QM/MM border); otherwise (e.g., for the DNA–enzyme complex), the QM region is saturated by hydrogen atoms (see section 4 for details).

The present study restricts itself on the size convergence for single snapshots of each molecular system (for reasons of computational expense). However, the results are averaged over all central atoms (of each atom type), to provide a more general picture of size convergence (see section 5.1.1).

To access QM regions with up to roughly 1500 atoms, the present study restricts to GIAO-HF/DFT levels and mainly applies basis sets such as 6-31G\*\*<sup>20,21</sup> and SVP,<sup>22</sup> while larger basis sets are employed only for comparison in the amino-pyrazole system for selected QM sizes with up to 827 atoms (9036 basis functions). For the methods and basis sets such as 6-31G\*\* and SVP, errors of absolute isotropic constants can be rather large, although NMR shifts relative to the respective reference molecules (e.g., tetramethylsilane) have shown to be less sensitive (see section 5.1.4). Even more so, for the present study of convergence with QM size, only relative changes of the isotropic shieldings toward the calculation with largest QM region are considered. We will show below that the convergence behavior is widely invariant to the methods and basis sets employed (sections 5.1.2 and 5.1.3). All calculations are performed with a development version of the Q-Chem program package<sup>23</sup> based on the recently introduced DL-CPSCF method<sup>5</sup> with sufficiently tight thresholds for SCF and CPSCF convergence, integral threshold, and verified accuracy of the chosen Laplace expansion.

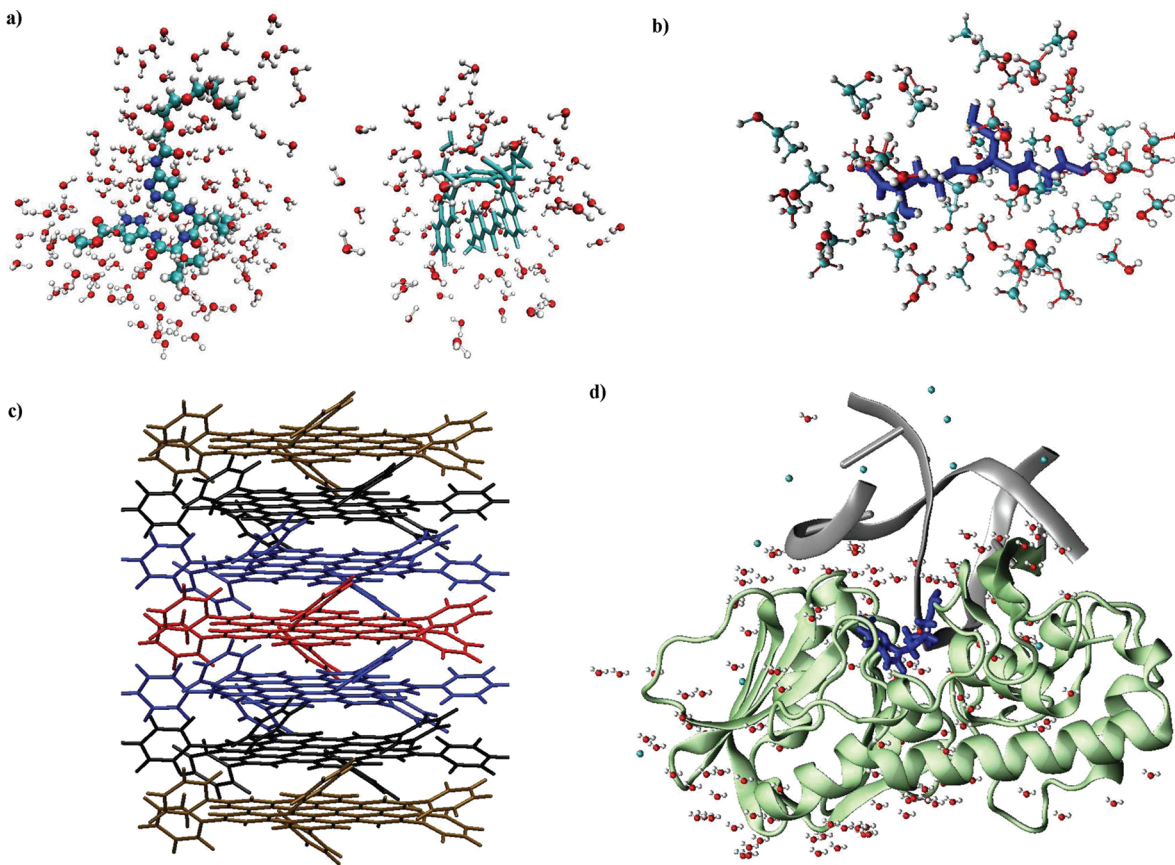


**Figure 2.** (a) Aminopyrazole peptide<sup>24</sup> (left) and molecular clip (right) in water<sup>25</sup> shown exemplarily inside a water environment of 5 Å (the largest considered QM spheres included up to 10 Å of the environment). (b) Glutathione<sup>26</sup> shown exemplarily inside a methanol environment of 5 Å (the largest considered QM spheres included up to 10 Å of the environment). (c) Heptamer cutout of the columnar structure of phenyl-substituted hexa-peri-hexabenzocoronenes.<sup>28</sup> (d) Complex of MutM enzyme (green) and DNA (gray) containing an 8-Oxo-G lesion (blue).<sup>27,30</sup>

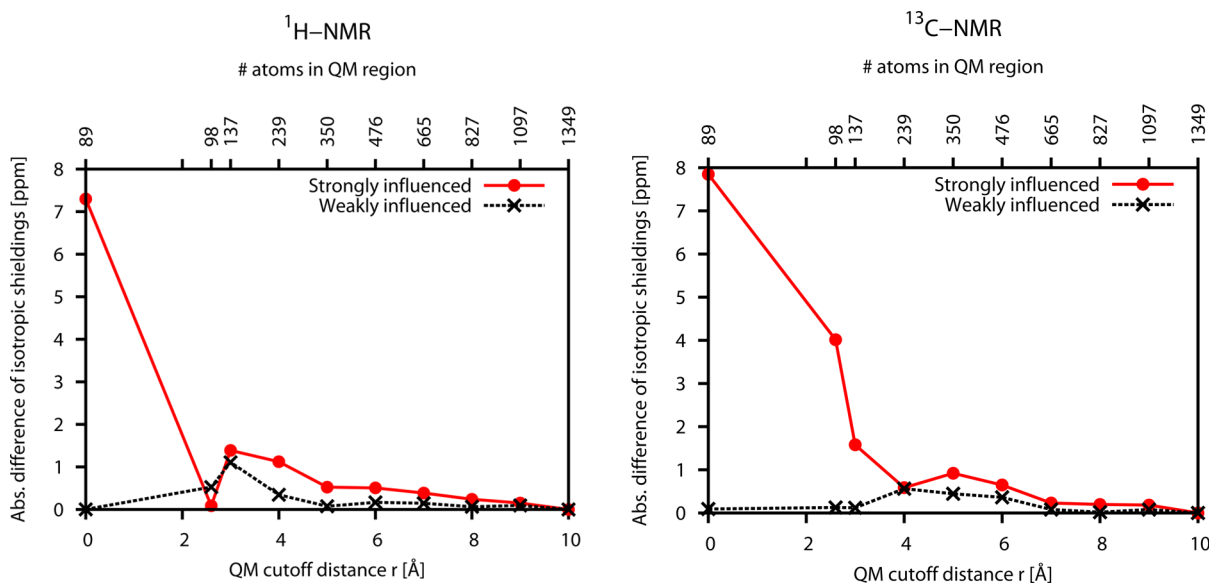


**Figure 3.** Absolute value of the difference in isotropic shieldings with respect to the result obtained for the largest QM region ( $r = 10 \text{ \AA}$ ) for the most and least influenced  $^1\text{H}$  and  $^{13}\text{C}$  nucleus of aminopyrazole in water, pure QM: GIAO-B3LYP/SVP.

#### 4. MOLECULAR SYSTEMS

For the present study, we consider various selected molecular systems (Figure 2):

- aminopyrazole in aqueous solution<sup>24</sup>
- molecular clip in aqueous solution<sup>25</sup>

- glutathione in methanol<sup>26</sup>
- DNA–enzyme complex<sup>30</sup>
- solid-state hexa-peri-hexabenzocoronenes<sup>28</sup>

The first two examples are aqueous solute systems: Starting from the solute molecule in the vacuum, more and more of the

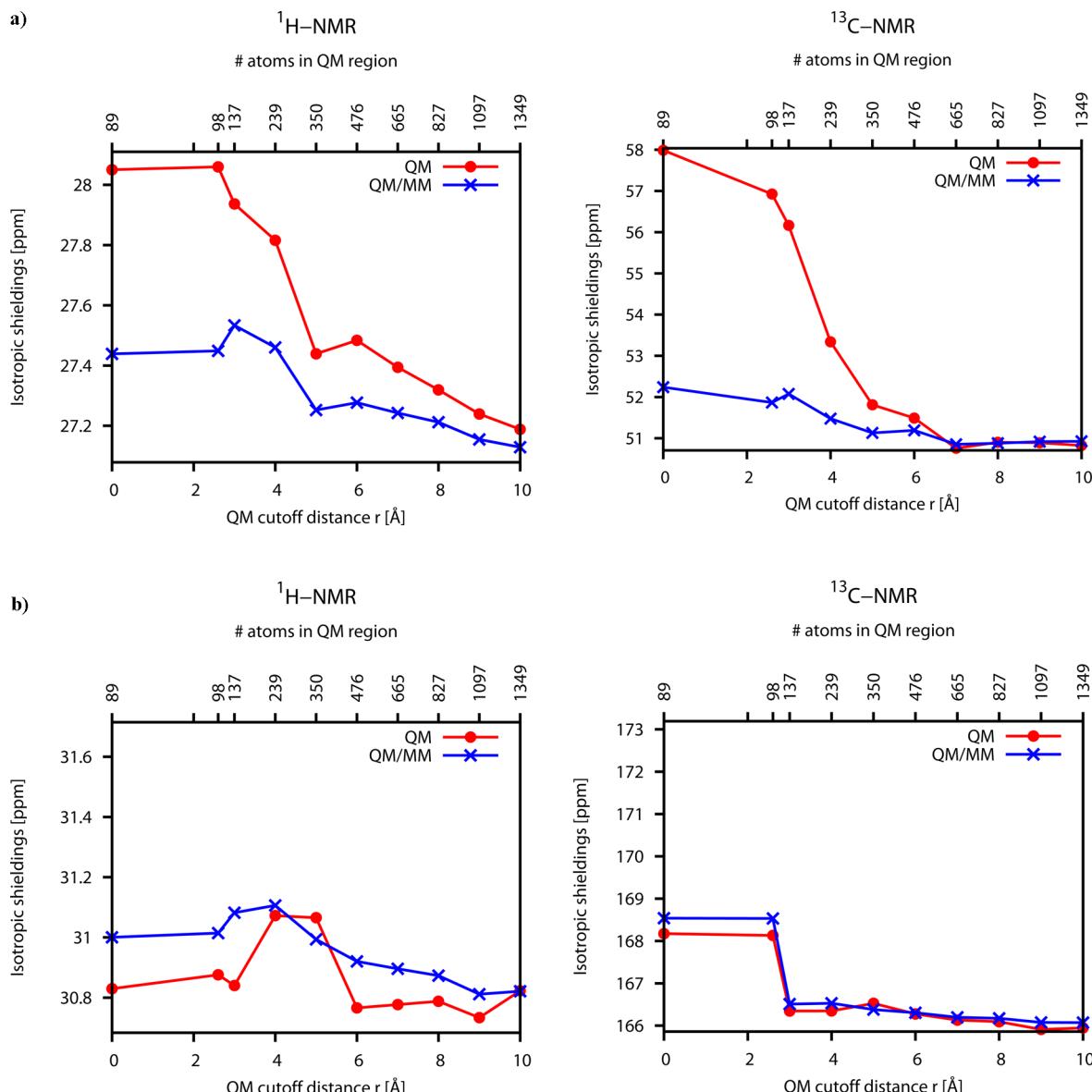


**Figure 4.** (a) Isotropic shieldings for selected nuclei in the aminopyrazole, where the benefit of QM/MM as compared to pure QM is (a) best and (b) worst, respectively, for  $^1\text{H}$  and  $^{13}\text{C}$  (GIAO-B3LYP/SVP).

water environment is explicitly treated by QM. The remaining part of the molecular system is then incorporated within the QM/MM approach based on a TIP3P<sup>29</sup> model of water. To avoid covalent bond cleavage at the QM/MM border, water molecules, which were not fully inside the actual QM region according to the QM cutoff distance (see section 3), are excluded from the actual QM region and are treated quantum-mechanically only for the next larger QM sizes.

**4.1. Aminopyrazole in Aqueous Solution.** For the example of an aminopyrazole peptide in water,<sup>24</sup> the monomer structure was extracted from the crystal structure of the hexamer. The monomer was optimized in vacuo by means of MP2/6-31G\*\* (frozen-core), and subsequently it was surrounded by a water sphere (50 Å), which was then relaxed by means of a molecular dynamics (MD) simulation (300 K, equilibrium 1 ps, total time 20 ps, step 1.5 fs) using the Merck Molecular Force Field (MMFF94<sup>31</sup>) for frozen positions of the solute within the Macromodel package.<sup>32</sup> The last MD snapshot with a total system of 3359 atoms was cut out, comprising the aminopyrazole and

15 Å of the surrounding water. For the convergence study, up to 1367 QM atoms were included within the QM region.

**4.2. Molecular Clip in Aqueous Solution.** A second example was prepared starting from the optimized host–guest complex of a naphthalene clip as specified in ref 25 (rests R = P(CH<sub>3</sub>)O<sub>2</sub>CH<sub>3</sub>; guest = N-methylnicotinamide). The water environment was set up analogously to the first example. Here, the total system comprises 3241 atoms, and the largest QM cutout for the convergence study consists of 1150 atoms.

**4.3. Glutathione in Methanol.** A third example considers the convergence behavior for another polar solvent: The ideal structure of the tripeptide glutathione (PDB code 1DUG<sup>26</sup>) is embedded into a methanol environment (50 Å) with the aid of the Desmond system builder of the Maestro Schroedinger suite.<sup>33</sup> Subsequently, an MD simulation using the Merck Molecular Force Field (MMFF94<sup>31</sup>) within the Macromodel package<sup>32</sup> is performed for the methanol solvent (300 K, equilibrium 1 ps, total time 20 ps, step 1.5 fs), while the nuclear positions of the solute are frozen. The last snapshot was taken

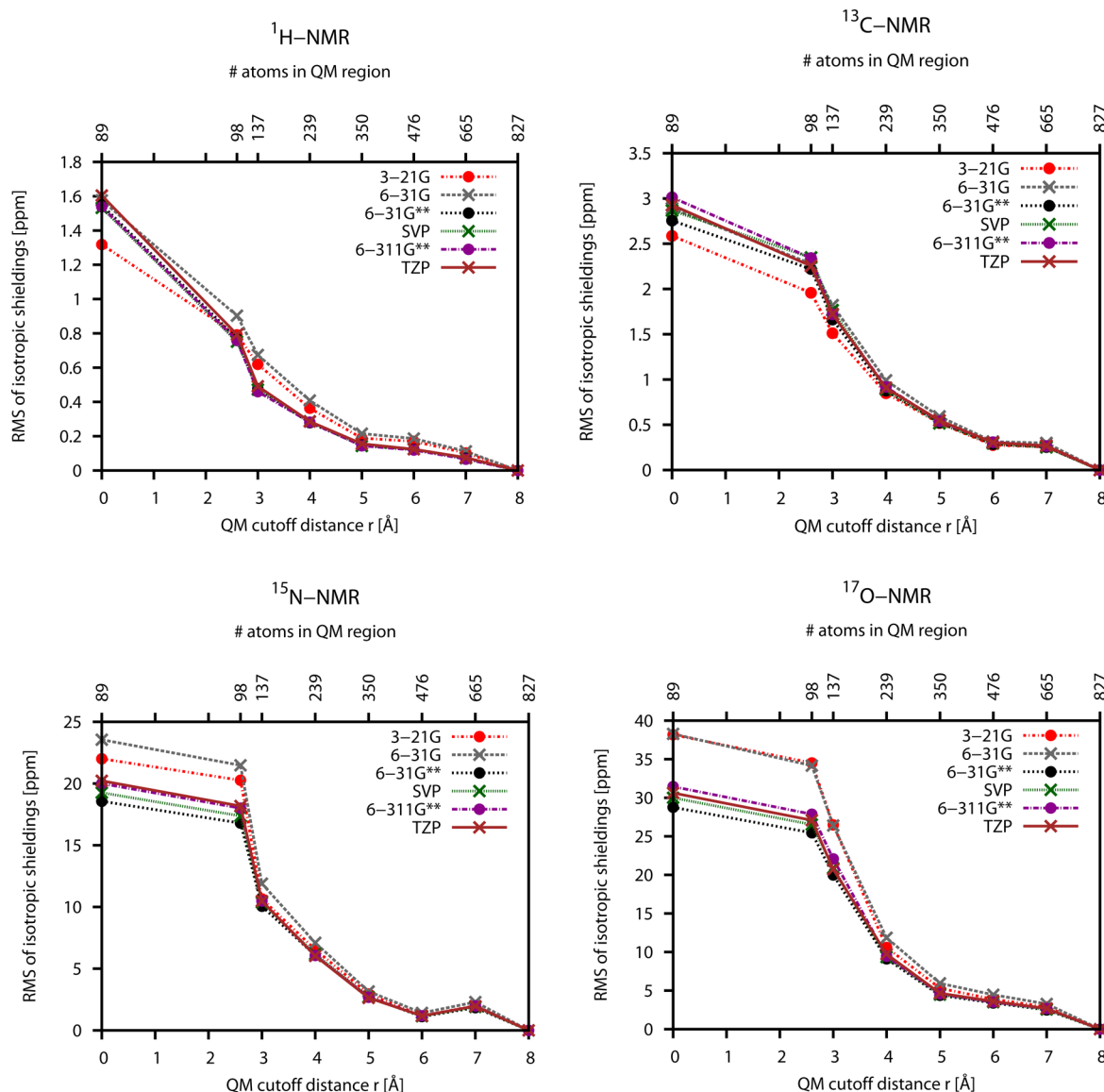


**Figure 5.** Root mean square deviations of isotropic shieldings with respect to the QM result with the largest QM cutoff distance (here 8 Å) for different basis sets over 44  $^1\text{H}$ , 27  $^{13}\text{C}$ , 9  $^{15}\text{N}$ , and 9  $^{17}\text{O}$  nuclei, pure QM: GIAO-HF.

for the QM/MM study. For the QM/MM partitioning, it is taken care that no covalent bonds of a solvent molecule at the QM/MM border are broken, in accordance with the previous examples. Point charges of methanol for the QM/MM calculations are extracted from the MMFF94 parameter sets. For this example, the total system consists of 2059 atoms and the largest QM cutout of 961 atoms.

**4.4. DNA Enzyme Complex.** For the previous examples, the solute presents the central region of atoms, for which the knowledge of NMR shieldings is of special interest. Likewise, in DNA–protein complexes, the main focus of interest is for many cases on a limited molecular region. For example, in studying the enzymatic DNA repair (see, for example, refs 30, 27), the main focus of attention can be on a single DNA lesion and the influence of the surrounding residues. As an example, we study here a DNA–protein complex containing a single oxidative lesion, 8-Oxo-G, based on the crystal structure with the PDB code 1R2Y.<sup>27</sup>

We employ standard AMBER parameters (FF-10) for DNA, protein residues, and water molecules and parameters from ref 34 for the 8-Oxo-G lesion. The crystal structure is saturated with

hydrogen atoms and neutralized by  $\text{Na}^+$  counterions. Subsequently, the positions of hydrogens are optimized by means of the NAMD force field engine.<sup>35</sup> The total system without extra water molecules comprises 5515 atoms. Additionally, a water sphere of 20 Å was added to the structure, minimized ( $10^5$  steps), and relaxed by means of an MD simulation (298 K, step 1.0 fs, 0.1 ns). A cutout from the last MD conformation of the DNA enzyme with 15 Å of the environment was taken as total system in water solvent (30647 atoms). For the convergence study, more and more of the surrounding protein residues and DNA residues (5'-nucleotides) are included within the QM region up to 1752 QM atoms. Unlike for the previous examples, covalent bond breaks cannot be avoided, when the QM region is cut out for the convergence study. Therefore, with the aid of the ChemShell program,<sup>36</sup> broken bonds at the intersection are saturated by hydrogen atoms. MM point charges close to the intersection are adjusted according to refs 36 and 37.

**4.5. Solid-State Hexa-peri-hexabenzocoronenes.** A last example focuses on a molecular system, for which environmental effects are dominated by ring currents of neighboring aromatic

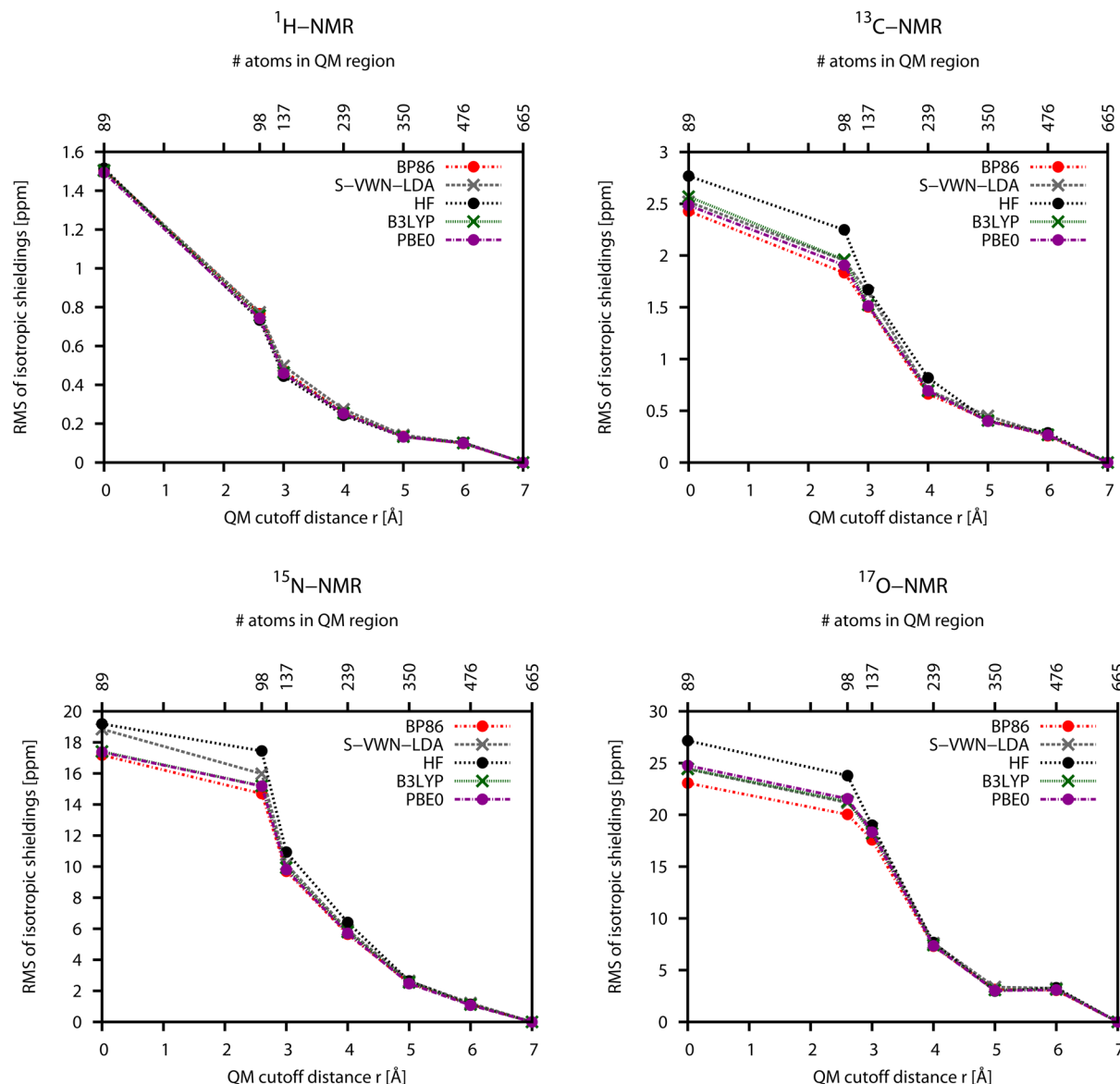


**Figure 6.** Root mean square deviations of isotropic shieldings with respect to the QM result with the largest QM cutoff distance (here 7 Å) for different QM methods over 44  $^1\text{H}$ , 27  $^{13}\text{C}$ , 9  $^{15}\text{N}$ , and 9  $^{17}\text{O}$  nuclei. QM part: GIAO with 6-31G\*\* basis.

cycles and a minor role of electrostatic effects is expected. In this respect, the influence of neighboring rings (stacking distance 3.5 Å) in the columnar structure of phenyl-substituted hexaperi-hexabenzocoronene (HBC<sup>28</sup>) onto a central unit is studied. As the reference system, the heptamer was chosen for both pure QM and QM/MM. For the case of QM/MM calculations, the external point-charges were determined by the model of restrained electrostatic potentials<sup>38</sup> for the monomer.

## 5. RESULTS

The key aspects of the evaluation procedure concerning the statistical evaluation of results for individual nuclei, dependency on the basis set, dependency on the QM method, and benchmark criteria are discussed in the following for the example of the aminopyrazole in aqueous solution. Subsequently, sections 5.2–5.5 summarize the results for the other investigated systems according to the proposed evaluation procedure for  $^1\text{H}$  and  $^{13}\text{C}$  nuclei.

In addition, the Supporting Information provides for all molecular systems various additional diagrams for maximum

deviations, best and worst performance of QM/MM versus pure QM, and also information for nitrogen and oxygen nuclei (if contained in the chemical system).

### 5.1. Results for Aminopyrazole in Aqueous Solution.

**5.1.1. Statistical Evaluation.** Regarding the study of size convergence, the results for the individual central nuclei need to be evaluated statistically to draw more general conclusions for two main reasons: First, one needs to account for the fact that the nuclei of the central molecular region are influenced to different extents by the chemical environment due to their specific bonding situation. Second, the quality of a description by MM schemes can vary strongly for individual nuclei.

The first aspect, the different extent of environmental effects, is illustrated in Figure 3. The convergence of the isotropic shielding toward the result of the calculation with the largest QM region is shown for the most and least influenced  $^1\text{H}$  and  $^{13}\text{C}$  nuclei in the aminopyrazole molecule: The change of gas-phase values with the surrounding radius  $r = 0$  by the environmental effects in our present system spans from 7.2 to 0.1 ppm for  $^1\text{H}$  and from 7.9 to 0.0 ppm for  $^{13}\text{C}$ .

**Table 1.**  $^1\text{H}$  NMR Shifts<sup>a</sup> (in ppm) at GIAO-HF, -DFT, and -MP2 Levels With Respect to  $\text{CH}_4$ <sup>b</sup> and the Mean Deviation  $\Delta$  and Sample Standard Deviation  $\Delta_{\text{std}}$  With Respect to CCSD(T) Results

molecule	HF	B3LYP <sup>42,43</sup>	BP86 <sup>41</sup>	B97-2 <sup>61</sup>	PBE <sup>62</sup>	PBE0 <sup>44</sup>	B3LYP <sub>GGA</sub> <sup>0.05 63</sup>	KT2 <sup>64</sup>	MP2	CCSD(T)
$\text{CH}_3\text{CH}_3$	0.41	0.66	0.73	0.63	0.78	0.64	0.73	0.74	0.57	0.56
$\text{CH}_2\text{CH}_2$	5.37	5.61	5.77	5.63	5.60	5.74	5.45	5.57	5.22	5.13
CHCH	1.20	1.03	1.06	1.08	1.28	1.10	1.13	1.20	1.19	1.14
$\text{CH}_3\text{CH}_2\text{CH}_3$	0.62	1.15	1.29	1.11	1.32	1.14	1.27	1.48	1.09	1.05
$\text{CH}_3\text{CH}_2\text{CH}_2$	0.49	0.72	0.81	0.69	0.83	0.71	0.80	0.81	0.65	0.63
$\text{CH}_2(\text{CH})_2\text{CH}_2$ (cis)	5.00	5.26	5.42	5.29	5.24	5.39	5.13	5.14	5.00	4.86
$\text{CH}_2(\text{CH})_2\text{CH}_2$ (trans)	4.93	5.12	5.29	5.17	5.08	5.27	5.00	5.10	4.96	4.81
$\text{CH}_2(\text{CH})_2\text{CH}_2$	6.27	6.42	6.57	6.43	6.44	6.54	6.22	6.33	6.17	6.02
$\text{C}_6\text{H}_6$	7.20	7.34	7.46	7.38	7.29	7.49	7.15	7.18	7.34	7.08
$\Delta$	-0.02	-0.20	-0.31	-0.21	-0.26	-0.27	-0.16	-0.23	-0.08	
$\Delta_{\text{std}}$	0.21	0.19	0.25	0.21	0.14	0.25	0.11	0.15	0.08	

<sup>a</sup>Basis set 6-311G\*\* and geometries according to ref 45, where HF, B3LYP, and MP2 data have also been listed. <sup>b</sup>The absolute isotropic shieldings of  $\text{CH}_4$  (in ppm) are 31.87 [HF], 31.91 [B3LYP], 31.88 [BP86], 31.86 [B97-2], 32.06 [PBE], 31.78 [PBE0], 31.86 [B3LYP<sub>GGA</sub><sup>0.05</sup>], 31.70 [KT2], 31.78 [MP2], 31.85 [CCSD(T)].

**Table 2.**  $^{13}\text{C}$  NMR Shifts<sup>a</sup> (in ppm) at GIAO-HF, -DFT, and -MP2 Levels With Respect to  $\text{CH}_4$ <sup>b</sup> and the Mean Deviation  $\Delta$  and Sample Standard Deviation  $\Delta_{\text{std}}$  With Respect to CCSD(T) Results

molecule	HF	B3LYP <sup>42,43</sup>	BP86 <sup>41</sup>	B97-2 <sup>61</sup>	PBE <sup>62</sup>	PBE0 <sup>44</sup>	B3LYP <sub>GGA</sub> <sup>0.05 63</sup>	KT2 <sup>64</sup>	MP2	CCSD(T)
$\text{CH}_3\text{CH}_3$	11.7	16.1	16.3	14.7	16.8	14.8	17.3	17.0	13.5	13.0
$\text{CH}_3\text{F}$	71.1	83.0	84.6	79.6	85.3	81.1	84.2	82.0	79.6	76.3
$\text{CH}_3\text{OH}$	52.0	62.3	63.7	59.4	64.2	60.3	63.9	62.8	59.2	56.5
$\text{CH}_3\text{NH}_2$	32.0	39.7	40.5	37.5	41.1	37.9	41.3	40.8	36.6	35.0
$\text{CH}_3\text{CHO}$	33.5	41.8	42.8	39.1	43.6	40.7	42.9	41.5	38.6	36.9
$\text{CH}_3\text{COCH}_3$	32.2	39.3	40.2	37.1	40.6	38.6	40.2	38.3	37.0	35.4
$\text{CH}_3\text{CN}$	4.9	9.3	10.3	8.9	10.6	9.1	10.5	10.6	7.9	7.7
CO	225.1	211.5	204.6	206.9	206.3	213.2	193.3	187.9	190.6	194.2
$\text{CO}_2$	148.0	143.0	138.7	139.5	139.6	143.0	138.2	134.1	138.1	139.4
CF4	116.3	142.9	146.4	137.1	147.3	139.6	148.5	140.1	136.9	132.7
HCN	127.7	122.6	120.0	120.4	121.0	124.6	116.1	110.9	114.4	113.7
$\text{CH}_2\text{CH}_2$	135.8	140.9	140.0	136.4	140.9	140.8	135.2	130.6	130.3	126.6
CHCH	81.8	83.4	82.9	80.8	84.0	85.0	82.2	76.6	78.2	76.3
$\text{CH}_3\text{CHO}$	211.4	218.8	216.8	212.0	218.0	217.7	208.0	202.0	200.3	198.6
$\text{CH}_3\text{COCH}_3$	218.9	225.3	222.1	217.7	223.0	223.0	214.7	207.8	207.4	205.7
$\text{CH}_3\text{CN}$	135.2	132.3	129.5	129.2	130.6	133.1	126.0	121.0	125.5	122.5
$\text{CH}_2\text{CCH}_2$	81.7	85.1	84.5	83.0	85.1	85.3	82.0	78.5	80.6	79.3
$\text{CH}_2\text{CCH}_2$	240.0	241.4	235.3	232.7	236.1	238.2	228.0	221.8	227.5	220.5
$\text{C}_6\text{H}_6$	140.7	144.6	142.2	139.2	143.2	143.3	139.3	133.2	137.6	134.8
$\text{CH}_2\text{O}$	204.9	215.1	215.2	208.7	216.9	215.3	204.1	199.5	194.7	192.6
$\Delta$	-5.1	-9.6	-8.5	-5.8	-9.4	-8.9	-5.6	-1.9	-1.8	
$\Delta_{\text{std}}$	10.5	6.9	6.0	4.9	6.3	6.9	4.1	3.9	2.1	

<sup>a</sup>Basis set qz2p and geometries according to ref 46, where HF and MP2 data have also been listed. <sup>b</sup>The absolute isotropic shieldings of  $\text{CH}_4$  (in ppm) are 195.7 [HF], 189.7 [B3LYP], 190.7 [BP86], 192.6 [B97-2], 191.8 [PBE], 193.9 [PBE0], 194.6 [B3LYP<sub>GGA</sub><sup>0.05</sup>], 198.4 [KT2], 201.5 [MP2], 199.5 [CCSD(T)].

The second aspect, that is, the different individual benefit by a QM/MM description as compared to pure QM, turns out to be also very distinctive in all molecular systems. In Figure 4, the case where one benefits most from the QM/MM description is compared to the case of lowest benefit for the example of individual nuclei in the aminopyrazole. While according to Figure 4a the inclusion of the environment by means of QM/MM seems to highly pay off, one would see no benefit of QM/MM as compared to pure QM according to Figure 4b (actually, for the lowest QM spheres, the QM/MM results are for the selected single cases even slightly worse than pure QM results, indicating a failure of the standard MM parameters for the specific bonding situation). Details of how the case of best and worst performances have been selected are described in the Supporting Information.

Therefore, to get a more general picture of how large the QM region needs to be for a desired accuracy and also of how the inclusion of MM by means of QM/MM influences the convergence behavior, root-mean-square deviations over all central nuclei (of each type) are taken for all of the following results, according to the equation:

$$\text{RMS}(r) = \sqrt{\frac{\sum_A^N \{\sigma_A(r) - \sigma_A^{\text{QM/MM}}(r_{\max})\}^2}{N}} \quad (8)$$

Here, the sum runs over all  $N$  nuclei of each type (e.g.,  $^1\text{H}$ ), and  $\sigma_A$  denotes the isotropic shielding of a central atom, calculated either at pure QM or at QM/MM level. According to sections 3 and 4, the distance  $r$  specifies the size of the QM sphere around the central molecular region, and  $r_{\max}$  is the size of the largest

considered QM sphere. Note that both the QM/MM and the pure QM calculations employ as reference the largest QM/MM calculation, because this is expected to be most accurate. Thus, if the largest pure QM and QM/MM calculations still differ due to a remaining MM part, the RMS of the largest pure QM calculation can be different from zero.

**5.1.2. Dependency on Basis Set.** To reach convergence with QM size, rather large QM regions are required (as discussed later in detail), which limits the affordable basis set sizes. Therefore, the influence of the basis set on size convergence is investigated in Figure 5 for the example of the aminopyrazole (at HF level). The major differences occur for the smaller QM spheres, especially for the smallest basis sets 3-21G and 6-31G without polarization functions, while the long-range behavior is almost exactly reproduced already for these smallest basis sets. Hence, for the following evaluation of size convergence, we restrict ourselves to the SVP and 6-31G\*\* basis sets.

**5.1.3. Dependency on QM Method.** Another important aspect is the influence by the chosen QM method. Figure 6 compares HF results with several DFT functionals.<sup>39–44</sup> A

comparison to other correlation methods, such as MP2, would be desirable, but the computational effort is too high with the currently available methods due to the required large system sizes. Nevertheless, like for the basis set dependency, the major (but still small) differences of HF and DFT results occur for the smaller QM spheres and for the heavier atoms. The general picture of the convergence behavior is the same for all considered methods, and therefore the following convergence studies are performed at HF or B3LYP level.

**5.1.4. Benchmark Criteria.** The QM region was increased to a QM cutoff distance of around 10 Å, where the deviations typically fall below 0.1/0.2 ppm for <sup>1</sup>H/<sup>13</sup>C (see details below). In the following sections, the required QM sizes for any looser criterion can be extracted from the corresponding figures of RMS deviations as a function of the QM size. However, for an explicit discussion in the following text, we choose only one example accuracy value. Our example is geared to the error of GIAO-HF/DFT levels, as for large system sizes applications are so far mainly limited to such levels of QM theory (although we expect that our findings concerning

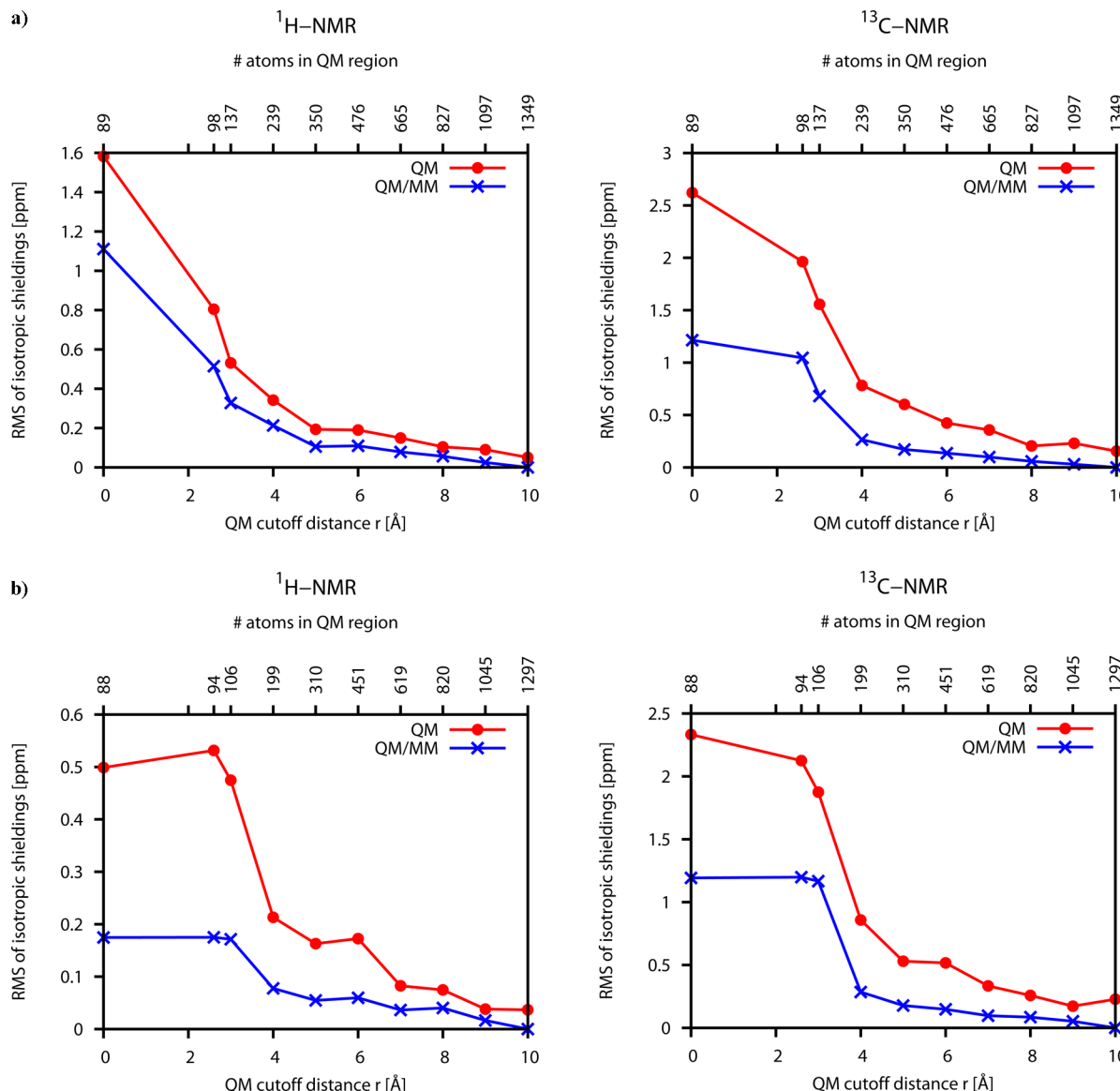


Figure 7. continued

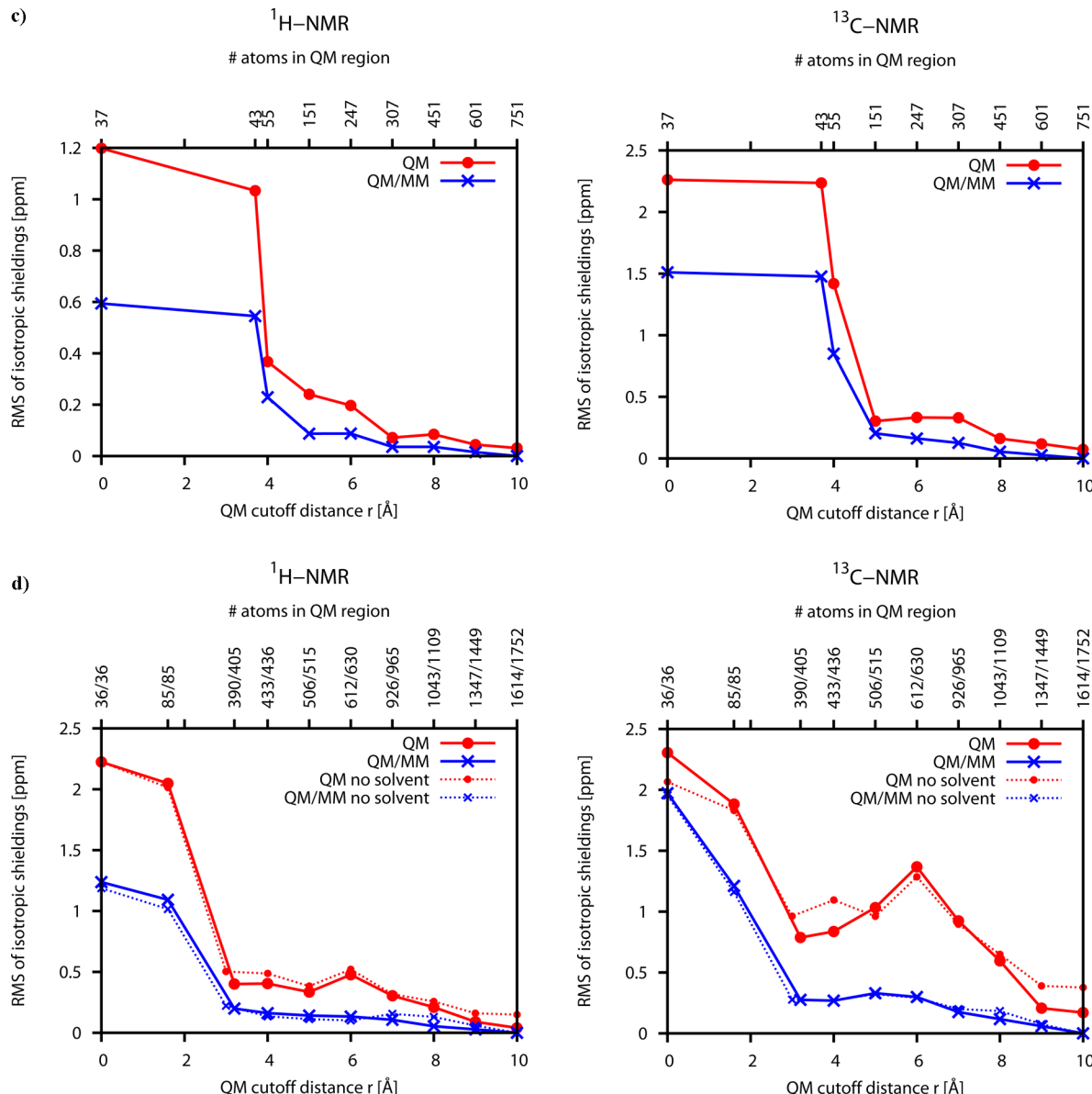


Figure 7. continued

required QM sizes would also hold for higher level QM methods as discussed in the preceding sections).

The accuracy of isotropic NMR shieldings has been studied in several comprehensive publications (see, e.g., refs 45–58). In Tables 1 and 2, we present data for HF, several DFT functionals, and MP2 for small molecules, for which also measurements in the gas phase are available<sup>45,52,59</sup> (for a closely related discussion, see refs 46 and 52). The geometries were chosen as specified in refs 45 and 46 for  $^1\text{H}$  and  $^{13}\text{C}$ , and the MP2 and CCSD(T) data have been calculated with the help of the CFOUR program.<sup>60</sup> The sample standard deviation  $\Delta_{\text{std}}$  (as an approximate average measure for the accuracy of relative isotropic shieldings) with respect to the CCSD(T) data reaches for  $^1\text{H}/^{13}\text{C}$  from 0.25/10.5 ppm to 0.11/3.9 ppm in case of HF or DFT and to 0.08/2.1 ppm in case of MP2.

Furthermore, from the calculated data of Table 2, one can also deduce that for a selection of chemically related structures, the standard deviations are considerably lower for all methods. For example, the standard deviation for carbon within a methyl

group bound to different substituents ( $-\text{H}$ ,  $-\text{CH}_3$ ,  $-\text{F}$ ,  $-\text{OH}$ ,  $-\text{NH}_2$ ,  $-\text{CHO}$ ,  $-\text{COCH}_3$ ,  $-\text{CN}$ ) is between 2.2 and 1.1 ppm for HF/DFT and 1.2 ppm for MP2 (values are not explicitly shown in Table 2). By this, another possibility for improving the accuracy of NMR chemical shifts is illustrated: the concept of intermediate references (see, e.g., refs 65 and 66). The shift toward a standard reference molecule (e.g., tetramethylsilane) is calculated by a higher level QM method (e.g., MP2) for a smaller molecular cutout of the region of interest. The effects due to the specific conformation and/or the environment are then included as increments calculated at a lower QM level. By this, we expect that the accuracies of  $^{13}\text{C}$  shifts can be improved to about 2–3 ppm for GIAO-DFT methods and smaller basis sets. Assuming that an additional error of 20% (at the worst) due to neglecting environmental effects is acceptable, one obtains a value of 0.5 ppm as a reasonable example threshold for  $^{13}\text{C}$ .

In addition to the example benchmark of 0.1/0.5 ppm for the nuclei  $^1\text{H}/^{13}\text{C}$ , the ratios  $\text{RMS}^{\text{QM}}/\text{RMS}^{\text{QM/MM}}$  for each QM size are computed and averaged over all considered QM sizes

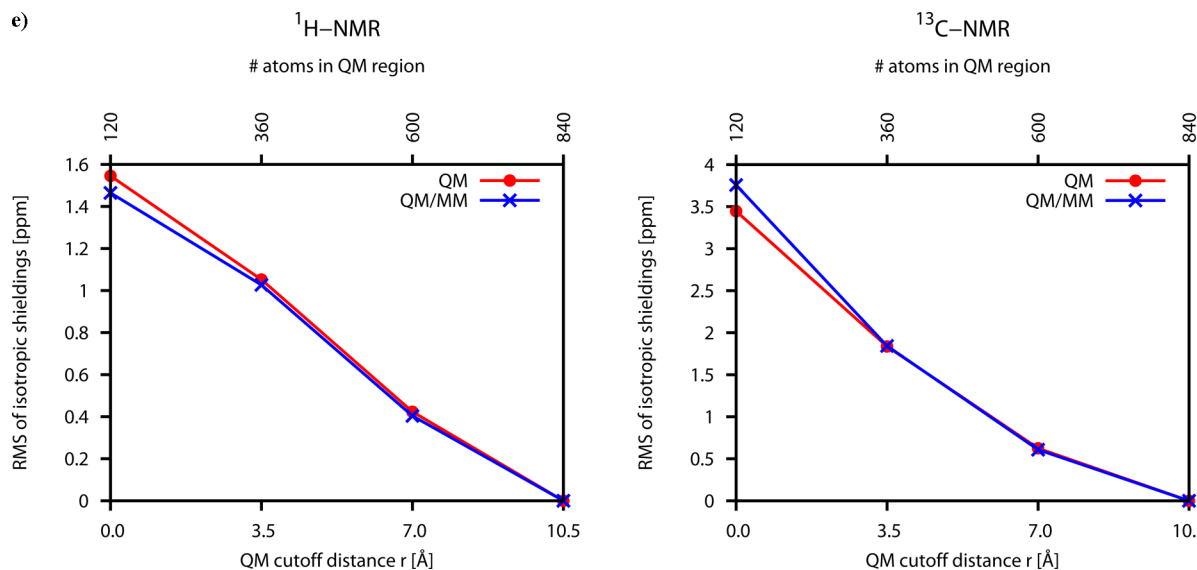


**Figure 7.** Root mean square deviations of isotropic shieldings with respect to the QM/MM result with the largest QM cutoff distance in case of pure QM and QM/MM for: (a) aminopyrazole in water over 44 <sup>1</sup>H and 27 <sup>13</sup>C nuclei (GIAO-B3LYP/6-31G\*\*), (b) molecular clip in water over 36 <sup>1</sup>H and 41 <sup>13</sup>C nuclei (GIAO-HF/6-31G\*\*), (c) glutathione in methanol over 17 <sup>1</sup>H and 10 <sup>13</sup>C nuclei (GIAO-B3LYP/SVP), (d) DNA–protein complex over 11 <sup>1</sup>H and 10 <sup>13</sup>C nuclei (GIAO-HF/6-31G\*\*); here, the dotted lines refer to calculations without an additional water environment (see section 4 for details), (e) hexa-peri-hexabenzocoronenes over 42 <sup>1</sup>H and 78 <sup>13</sup>C nuclei (GIAO-HF/6-31G\*\*); the points at 3.5, 7.0, and 10.5 Å refer to the trimer, pentamer, and heptamer cutout, respectively.

(except the largest QM size, to avoid division by zero) to measure the overall benefit of QM/MM as compared to pure QM. The resulting single measure is hereafter denoted as mean efficiency number of QM/MM and illustrates how strongly the RMS error is typically reduced by QM/MM versus pure QM.

**5.1.5. Convergence Results for Aminopyrazole in Aqueous Solution.** Figure 7a shows the results for the aminopyrazole peptide in water. The deviations fall below 0.1/0.5 ppm for <sup>1</sup>H/<sup>13</sup>C at a QM cutoff distance of 9.0 Å (1097 atoms)/6.0 Å (476 atoms) in case of pure QM as compared to 7.0 Å (665 atoms)/4.0 Å (239 atoms) in case of QM/MM. The mean efficiency number of QM/MM is 1.9/3.4 for <sup>1</sup>H/<sup>13</sup>C.

**5.2. Results for Molecular Clip in Aqueous Solution.** For the host–guest complex of the naphthalene clip, we follow the same path as above. The results are shown in Figure 7b. The deviations fall below 0.1/0.5 ppm for <sup>1</sup>H/<sup>13</sup>C at a QM cutoff distance of 7.0 Å (619 atoms)/7.0 Å (619 atoms) in case of pure QM as compared to 4.0 Å (199 atoms)/4.0 Å (199 atoms) in case of QM/MM. The mean efficiency number of QM/MM is 2.6/2.7 for <sup>1</sup>H/<sup>13</sup>C.

Thus, the general picture of size convergence in aqueous solutions is very similar to the first example, although some differences occur considering the hydrogen nuclei. Striving for an accuracy of 0.1 ppm, QM convergence is slightly faster in comparison with the aminopyrazole system. Second, the mean efficiency number of QM/MM is for the hydrogens somewhat larger than that for the hydrogens in the aminopyrazole system; that is, the benefit of QM/MM is slightly larger.

**5.3. Results for Glutathione in Methanol.** Figure 7c shows the results for the glutathione solute in methanol. The deviations fall below 0.1/0.5 ppm for <sup>1</sup>H/<sup>13</sup>C at a QM cutoff distance of 7.0 Å (307 atoms)/5.0 Å (151 atoms) in case of pure QM as compared to 5.0 Å (151 atoms)/5.0 Å (151 atoms) in case of QM/MM. The mean efficiency number of QM/MM is 2.2/2.3 for <sup>1</sup>H/<sup>13</sup>C. Hence, regarding the QM cutoff distances, the results resemble those obtained for the aqueous solutions. However, because the water environment is denser than the

methanol environment (both at 300 K), a specific QM cutoff distance corresponds to fewer atoms in methanol than in H<sub>2</sub>O.

**5.4. Results for DNA Enzyme Complex.** The results for the DNA enzyme complex are summarized in Figure 7d. The deviations fall below 0.1/0.5 ppm for <sup>1</sup>H/<sup>13</sup>C at a QM cutoff distance of 9.0 Å (1449 atoms)/9.0 Å (1449 atoms) in case of pure QM as compared to 8.0 Å (1109 atoms)/3.2 Å (405 atoms) in case of QM/MM. In addition to the solvated DNA–enzyme complex, also the results without solvent water are shown in Figure 7d by dotted lines. For the considered system, the convergence behavior remains very similar, with a marginally faster convergence for the pure QM calculations for the largest systems beyond 9 Å. For the smaller 3-21G basis set, the QM region was further enlarged to 13.0 Å (2379 atoms), where the deviation finally drops below 0.1 Å for <sup>1</sup>H also in case of pure QM and no water solvent (see the Supporting Information). The mean efficiency number of QM/MM is 2.7/3.4 for <sup>1</sup>H/<sup>13</sup>C.

**5.5. Results for Solid-State Hexa-peri-hexabenzocoronene.** Concerning the QM/MM benefit, the findings strongly change for the last considered test case (Figure 7e). The inclusion of electrostatic interactions by means of QM/MM hardly effects the results of pure QM (see Figure 7e). Therefore, and in light of the previous findings, one can conclude that in the HBC system the environmental effects are dominated by other effects that cannot be described by means of QM/MM, at least not within standard parametrization schemes. For the HBC system, influences are clearly dominated by aromatic ring currents. The remarkable long-range behavior was already described in refs 28, 67, and 68.

## 6. CONCLUSIONS

In our present work, we have investigated for several chemical systems and given conformations how the NMR shieldings of a central molecular region change if more and more of the environment is taken explicitly into account. In summary, one can conclude:

- For mean accuracies below 0.1/0.5 ppm for  $^1\text{H}/^{13}\text{C}$ , pure QM calculations need to include 6–10 Å of the environment around the considered nucleus.
- Therefore, roughly 300–1200 atoms need to be included for explicit descriptions of environmental effects by means of pure QM calculations for  $^1\text{H}/^{13}\text{C}$ .
- The benefit of conventional QM/MM schemes (here, electrostatic embedding based on external point charges) as compared to pure QM is mostly convincing and is shown to be rather invariant to the considered chemical systems with dominating electrostatic effects (mean efficiency numbers of QM/MM lie roughly between 2 and 4). Nevertheless, depending on the chemical system, QM regions with 200–1000 atoms are necessary for  $^1\text{H}/^{13}\text{C}$  for accuracies of 0.1/0.5 ppm.
- Smaller or no mean benefits of QM/MM can occur, if in particular effects other than electrostatic ones dominate, for example, aromatic ring currents.
- For individual nuclei, the benefit of QM/MM may be much larger, although in very few cases also a worsening of individual results due to QM/MM as compared to pure QM for the smallest QM regions is observed.

## ASSOCIATED CONTENT

### Supporting Information

Additional diagrams (maximum deviations, best and worst performance of QM/MM versus pure QM, information for nitrogen and oxygen shieldings) for all molecular systems and considered computational levels. Furthermore, detailed description of how the nuclei of best and worst performance have been selected. This material is available free of charge via the Internet at <http://pubs.acs.org>.

## AUTHOR INFORMATION

### Corresponding Author

\*E-mail: christian.ochsenfeld@uni-muenchen.de.

### Notes

The authors declare no competing financial interest.

## ACKNOWLEDGMENTS

We thank Dr. K. Sadeghian (LMU Munich) for help in preparing the DNA–protein structures and Dr. J. Kussmann (LMU Munich) for support concerning both structure preparation and calculations of NMR shielding tensors, in particular also for implementing further DFT functionals for the accuracy benchmark from the libxc library.<sup>69</sup> We thank Dr. Paul Sherwood (Daresbury Laboratory, U.K.) and Prof. Walter Thiel (MPI für Kohlenforschung, Germany) for the possibility to employ the ChemShell program suite. C.O. acknowledges financial support by the Volkswagen Stiftung within the funding initiative “New Conceptual Approaches to Modeling and Simulation of Complex Systems” and by the SFB 749 “Dynamik und Intermediate molekularer Transformationen” (DFG).

## REFERENCES

- (1) Kaupp, M.; Bühl, M.; Malkin, V. G. *Calculation of NMR and EPR Parameters, Theory and Applications*; Wiley-VCH: Weinheim, 2004.
- (2) Gauss, J. In *Modern Methods and Algorithms of Quantum Chemistry*; Grotendorst, J., Ed.; John von Neumann Institute for Computing: Jülich, 2000; Vol. 3, pp 541–592.
- (3) Ochsenfeld, C.; Kussmann, J.; Koziol, F. *Angew. Chem., Int. Ed.* **2004**, *43*, 4485–4489.
- (4) Kussmann, J.; Ochsenfeld, C. *J. Chem. Phys.* **2007**, *127*, 054103.
- (5) Beer, M.; Ochsenfeld, C. *J. Chem. Phys.* **2008**, *128*, 221102.
- (6) Beer, M.; Kussmann, J.; Ochsenfeld, C. *J. Chem. Phys.* **2011**, *134*, 074102.
- (7) Sherwood, P. In *Modern Methods and Algorithms of Quantum Chemistry*; Grotendorst, J., Ed.; John von Neumann Institute for Computing: Jülich, 2000; Vol. 3, pp 285–305.
- (8) Bakowies, D.; Thiel, W. *J. Phys. Chem.* **1996**, *100*, 10580–10594.
- (9) Senn, H. M.; Thiel, W. *Angew. Chem., Int. Ed.* **2009**, *48*, 1198–1229.
- (10) Lin, H.; Truhlar, D. *Theor. Chem. Acc.* **2007**, *117*, 185–199.
- (11) Hu, L.; Söderhjelm, P.; Ryde, U. *J. Chem. Theory Comput.* **2011**, *7*, 761–777.
- (12) Liao, R.-L.; Thiel, W. *J. Chem. Theory Comput.* **2012**, DOI: 10.1021/ct3000684.
- (13) Sebastiani, D.; Rothlisberger, U. *J. Phys. Chem. B* **2004**, *108*, 2807–2815.
- (14) Sumowski, C. V.; Ochsenfeld, C. *J. Phys. Chem. A* **2009**, *113*, 11734–11741.
- (15) Cui, Q.; Karplus, M. *J. Phys. Chem. B* **2000**, *104*, 3721–3743.
- (16) London, F. *J. Phys. Radium* **1937**, *8*, 397–409.
- (17) Ditchfield, R. *Mol. Phys.* **1974**, *27*, 789.
- (18) Wolinski, K.; Hinton, J. F.; Pulay, P. *J. Am. Chem. Soc.* **1990**, *112*, 8251–8260.
- (19) Ferré, N.; Ángyán, J. G. *Chem. Phys. Lett.* **2002**, *356*, 331–339.
- (20) Hehre, W. J.; Ditchfield, R.; Pople, J. A. *J. Chem. Phys.* **1972**, *56*, 2257–2261.
- (21) Hariharan, P. C.; Pople, J. A. *Theor. Chim. Acta* **1973**, *28*, 213–222.
- (22) Schäfer, A.; Horn, H.; Ahlrichs, R. *J. Chem. Phys.* **1992**, *97*, 2571–2577.
- (23) Development version of the program package Q-Chem, www.q-chem.com.
- (24) Rzepecki, P.; Hochdörffer, K.; Schaller, T.; Zienau, J.; Harms, K.; Ochsenfeld, C.; Xie, X.; Schrader, T. *J. Am. Chem. Soc.* **2008**, *130*, 586–591.
- (25) Klärner, F.-G.; Kahlert, B.; Nellesen, A.; Zienau, J.; Ochsenfeld, C.; Schrader, T. *J. Am. Chem. Soc.* **2006**, *128*, 4831–4841.
- (26) Ware, S.; Anderson, W. F.; Donahue, J. P.; Hawiger, J. *J. Protein Sci.* **1999**, *8*, 2663–2671.
- (27) Fromme, J. C.; Verdine, G. L. *J. Biol. Chem.* **2003**, *278*, 51543–51548.
- (28) Pisula, W.; Tomović, V.; Watson, M. D.; Müllen, K.; Kussmann, J.; Ochsenfeld, C.; Metzroth, T.; Gauss, J. *J. Phys. Chem. B* **2007**, *111*, 7481–7487.
- (29) Jorgensen, W. L.; Chandrasekhar, J.; Madura, J. D.; Impey, R. W.; Klein, M. L. *J. Chem. Phys.* **1983**, *79*, 926–935.
- (30) Coste, F.; Ober, M.; Carell, T.; Boiteux, S.; Zelwer, C.; Castaing, B. *J. Biol. Chem.* **2004**, *279*, 44074–44083.
- (31) Halgren, T. A. *J. Comput. Chem.* **1996**, *17*, 490–461.
- (32) Mohamadi, F.; Richards, N. G. J.; Guida, W. C.; Liskamp, R.; Lipton, M.; Caufield, C.; Chang, G.; Hendrickson, T.; Still, W. C. *J. Comput. Chem.* **1990**, *11*, 440–467.
- (33) *Desmond Molecular Dynamics System*; D. E. Shaw Research, Maestro-Desmond Interoperability Tools, version 2.4, New York, 2010.
- (34) Cheng, X.; Kelso, C.; Hornak, V.; de los Santos, C.; Grollman, A. P.; Simmerling, C. *J. Am. Chem. Soc.* **2005**, *127*, 13906–13918.
- (35) Phillips, J. C.; Braun, R.; Wang, W.; Gumbart, J.; Tajkhorshid, E.; Villa, E.; Chipot, C.; Skeel, R. D.; Kale, L.; Schulten, K. *J. Comput. Chem.* **2005**, *26*, 1781–1782.
- (36) Sherwood, P.; de Vries, A. H.; Guest, M. F.; Schreckenbach, G.; Catlow, C. R. A.; French, S. A.; Sokol, A. A.; Bromley, S. T.; Thiel, W.; Turner, A. J.; Billeter, S.; Terstegen, F.; Thiel, S.; Kendrick, J.; Rogers, S. C.; Casci, J.; Watson, M.; King, F.; Karlsen, E.; Sjøvoll, M.; Fahmi, A.; Schäfer, A.; Lennartz, C. *J. Mol. Struct. (THEOCHEM)* **2003**, *632*, 1–28.
- (37) de Vries, A. H.; Sherwood, P.; Collins, S. J.; Rigby, A. M.; Rigozzo, M.; Kramer, G. *J. Phys. Chem. B* **1999**, *103*, 6133–6141.

- (38) Bayly, C. I.; Cieplak, P.; Cornell, W.; Kollman, P. A. *J. Phys. Chem.* **1993**, *97*, 10269–10280.
- (39) Dirac, P. A. M. *Cambridge Philos. Soc.* **1930**, *26*, 376–385.
- (40) Vosko, S. H.; Wilk, L.; Nusair, M. *Can. J. Phys.* **1980**, *58*, 1200–1211.
- (41) Becke, A. D. *Phys. Rev. A* **1988**, *38*, 3098–3100.
- (42) Becke, A. D. *J. Chem. Phys.* **1993**, *98*, 1372–1377.
- (43) Stephens, P. J.; Devlin, F. J.; Chabalowski, C. F.; Frisch, M. J. *J. Phys. Chem.* **1994**, *98*, 11623–11627.
- (44) Adamo, C.; Scuseria, G. E.; Barone, V. *J. Chem. Phys.* **1999**, *111*, 2889–2899.
- (45) Zuschneid, T.; Fischer, H.; Handel, T.; Albert, K.; Häfleinger, G. *Z. Naturforsch.* **2004**, *59b*, 1153–1176.
- (46) Gauss, J. *J. Chem. Phys.* **1993**, *99*, 3629–3643.
- (47) Cheeseman, J. R.; Trucks, G. W.; Keith, T. A.; Frisch, M. J. *J. Chem. Phys.* **1996**, *104*, 5497–5509.
- (48) Olsson, L.; Cremer, D. *J. Chem. Phys.* **1996**, *105*, 8995–9006.
- (49) Adamo, C.; Barone, V. *Chem. Phys. Lett.* **1998**, *298*, 113–119.
- (50) Rablen, P. R.; Pearlmanand, S. A.; Finkbiner, J. *J. Phys. Chem. A* **1999**, *103*, 7357–7363.
- (51) Sun, H.; Sanders, L. K.; Oldfield, E. *J. Am. Chem. Soc.* **2002**, *124*, 5486–5495.
- (52) Auer, A. A.; Gauss, J.; Stanton, J. F. *J. Chem. Phys.* **2003**, *118*, 10407–10417.
- (53) Jensen, F. *J. Chem. Theory Comput.* **2008**, *4*, 719–727.
- (54) Zhao, Y.; Truhlar, D. G. *J. Phys. Chem. A* **2008**, *112*, 6794–6799.
- (55) Kongsted, J.; Aidar, K.; Mikkelsen, K. V.; Sauer, S. P. A. *J. Chem. Theory Comput.* **2008**, *4*, 267–277.
- (56) Mulder, F. A. A.; Filatov, M. *Chem. Soc. Rev.* **2010**, *39*, 578–590.
- (57) Gregušová, A.; Perera, S. A.; Bartlett, R. J. *J. Chem. Theory Comput.* **2010**, *6*, 1228–1239.
- (58) Kupka, T.; Stachów, M.; Nieradka, M.; Kaminsky, J.; Pluta, T. *J. Chem. Theory Comput.* **2010**, *6*, 1580–1589.
- (59) Jameson, A. K.; Jameson, C. *J. Chem. Phys. Lett.* **1987**, *134*, 461–466.
- (60) CFOUR, a quantum chemical program package written by: Stanton, J. F.; Gauss, J.; Harding, M. E.; Szalay, P. G. with contributions from Auer, A. A.; Bartlett, R. J.; Benedikt, U.; Berger, C.; Bernholdt, D. E.; Bomble, Y. J.; Christiansen, O.; Heckert, M.; Heun, O.; Huber, C.; Jagau, T.-C.; Jonsson, D.; Jusélius, J.; Klein, K.; Lauderdale, W. J.; Matthews, D. A.; Metzroth, T.; O'Neill, D. P.; Price, D. R.; Prochnow, E.; Ruud, K.; Schiffmann, F.; Stopkowicz, S.; Tajti, A.; Vázquez, J.; Wang, F.; Watts, J. D.; and the integral packages MOLECULE (Almlöf, J.; Taylor, P. R.), PROPS (Taylor, P. R.), ABACUS (Helgaker, T.; Jensen, H. J. Aa.; Jorgensen, P.; Olsen, J.), and ECP routines by Mitin, A. V.; van Wüllen, C. For the current version, see: <http://www.cfour.de>.
- (61) Wilson, P. J.; Bradley, T. J.; Tozer, D. *J. J. Chem. Phys.* **2001**, *115*, 9233–9242.
- (62) Perdew, J. P.; Burke, K.; Ernzerhof, M. *Phys. Rev. Lett.* **1996**, *77*, 3865–3868.
- (63) Helgaker, T.; Wilson, P. J.; Amos, R. D.; Handy, N. C. *J. Chem. Phys.* **2000**, *113*, 2983–2989.
- (64) Keal, T. W.; Tozer, D. *J. J. Chem. Phys.* **2003**, *119*, 3015–3024.
- (65) Ochsenfeld, C.; Koziol, F.; Brown, S. P.; Schaller, T.; Seelbach, U. P.; Klärner, F.-G. *Solid State Nucl. Magn. Reson.* **2002**, *22*, 128–153.
- (66) Zienau, J.; Kussmann, J.; Ochsenfeld, C. *Mol. Phys.* **2010**, *108*, 333–342.
- (67) Ochsenfeld, C. *Phys. Chem. Chem. Phys.* **2000**, *2*, 2153–2159.
- (68) Ochsenfeld, C.; Brown, S. P.; Schnell, I.; Gauss, J.; Spiess, H. W. *J. Am. Chem. Soc.* **2001**, *123*, 2597–2606.
- (69) Library of exchange-correlation functionals for density-functional theory (libxc), [www.tddft.org/programs/octopus/wiki/index.php/Libxc](http://www.tddft.org/programs/octopus/wiki/index.php/Libxc).